Check for updates

Suppression of the redox reaction between the IGZO surface and the reducing agent TMA using fluorine oxidizing agent treatment†

Yuseong Jang, [ID] Jinkyu Lee, Jinsung Mok, Junhyeong Park, [ID] Seung Yoon Shin and Soo-Yeon Lee [ID] *

We propose that the post-deposition oxidation of the IGZO surface is essential for improving the interface quality, with Al_2O_3 prepared by atomic layer deposition (ALD) employing a common metal precursor trimethylaluminum (TMA). Here, the ALD-Al_2O_3 process was conducted using H_2O as an oxidant at a substrate temperature of 150 °C after IGZO deposition. The depth-resolved X-ray photoelectron spectroscopy (XPS) and transmission electron microscopy (TEM) data reveal the defect-rich and poor interface of the standard Al_2O_3/IGZO stack due to the redox reaction between the IGZO surface and TMA. The anion character of the IGZO was modified by introducing fluorine, which is known as a stability enhancer for oxide semiconductors. We highlight that the presence of the fluorine also improves the interface quality with ALD-Al_2O_3. As a consequence of the fluorine incorporation prior to the ALD-Al_2O_3 process, the chemical reduction reaction of the IGZO surface was effectively alleviated, resulting in a defect-passivated and sharp interface owing to the strong oxidizing nature of the fluorine.

Introduction

CMOS (complementary metal-oxide semiconductor) compatibility, wide optical bandgap (>3.0 eV), and low-temperature processes have been driving InGaZnO (IGZO) thin-film transistors (TFTs) toward future electronic devices.[1–3] In particular, the low off-current of IGZO has attracted intensive efforts in both academia and industry for capacitor-less DRAM (dynamic random access memory) technology.[4–8] Undoubtedly, in the regulation of native defects of oxide semiconductors, oxygen vacancies (V_Os), have been the most important topic. In general, many studies have attempted to passivate the V_O by either cation or anion engineering. Cation doping, such as with Hf, can reduce the V_O concentration because of the strong metal–oxygen (M–O) bond strength.[9] It should be noted that the conduction band composed of large spherical s orbitals can be influenced depending on the cation dopant species. In terms of anion modification, the V_O states can be occupied by N, which has a higher orbital energy and larger ionic radius than O.[10] However, the metastability of metal nitride thin films remains to be addressed,[11] even though the M–N bond can be even stronger than the M–O bond based on thermodynamic calculations.[12] On the other hand, F is another promising element

because the smaller atomic radius and stronger electronegativity than O lead to V_O passivation and strong M–F bond formation.[13,14] Therefore, TFT stability is enhanced when F is incorporated into IGZO.[15–17] Furthermore, the presence of F reduces the vulnerability of IGZO to H penetration from plasma enhanced chemical vapor deposited (PECVD)-SiO_2.[18] The type and concentration of H species from the adjacent insulator are another major issue in discussing the device performance of IGZO TFT.[19] Therefore, attention should be paid to the gate insulator (GI) material, preparation, and process sequence. Atomic layer deposited Al_2O_3 (ALD-Al_2O_3) benefits from excellent step coverage, a low-temperature process, high-k, and large band offset with IGZO. In this regard, ALD-Al_2O_3 on IGZO (hereafter, ALD-Al_2O_3/IGZO stack) has been widely utilized in TFT configurations, where the Al_2O_3 functions as a top GI,[5,20–22] passivation layer,[23] and other functional layers.[24,25] However, there are several phenomena that should be addressed behind the ALD-Al_2O_3/IGZO stack. At the low substrate temperature of the ALD process, a large H concentration can be derived as a result of the incomplete combustion of hydroxyl groups,[26] so H diffusion into the underlying IGZO would be unavoidable. Moreover, the chemical reaction of the IGZO surface occurs during ALD-Al_2O_3, attributed to a common Al precursor, trimethylaluminum (TMA).[20] TMA is known to be a strong reducing agent,[27–29] which itself desires to be oxidized. The capability of TMA to reduce neighboring species has been the main cause of defect-rich interfaces, forming a two-dimensional electron gas (2DEG) between ALD-Al_2O_3 and bottom binary oxides such as TiO_2,[28,29] ZnO,[27,30] and In_2O_3.[31,32] Likewise, the

Department of Electrical and Computer Engineering, Inter-University Semiconductor Research Center, Seoul National University, 1 Gwanak-ro, Gwanak-gu, Seoul, 08826, Republic of Korea. E-mail: sooyeon.lee@snu.ac.kr

† Electronic supplementary information (ESI) available. See DOI: https://doi.org/10.1039/d3ra06768h

quaternary oxide IGZO was chemically reduced when exposed to the ALD-Al_2O_3 process, creating a defect-rich interface.[20] This chemical redox (oxidation–reduction) reaction should be alleviated for applications where a high quality ALD-Al_2O_3/IGZO interface is desired (e.g., capacitor-less DRAM or display devices using ALD-Al_2O_3/IGZO as a gate stack).

In this work, we demonstrate a top gate (TG) IGZO TFT with a channel length of 4 μm, where the IGZO channel and Al_2O_3 dielectric were prepared by radio-frequency (RF) magnetron sputtering and thermal ALD, respectively. The anion character of the IGZO was modified by introducing F, well-known as a stability enhancer for oxide semiconductors. The fluorine was incorporated using CF_4-based plasma treatment "after" IGZO deposition, namely fluorine "post"-deposition treatment (F-PDT). A low-temperature ALD process was employed to investigate if the presence of F can prohibit H diffusion during the ALD-Al_2O_3 process. Our main focus lies in the influence of F on the interface between ALD-Al_2O_3 and IGZO, which has rarely been examined. For this purpose, the depth-resolved X-ray photoelectron spectroscopy (XPS) data of all elements (Al, O, In, Ga, Zn, F, and C) obtained from the Al_2O_3 to IGZO are comprehensively presented. Combined with transmission electron microscopy (TEM) analysis, it could be seen that the F-PDT alleviated the chemical reduction reaction of the IGZO surface and, therefore, improved the interface quality with ALD-Al_2O_3. The electrical properties and negative bias stress (NBS) stability were enhanced, consistent with the XPS and TEM results. We believe that the post-deposition oxidation of IGZO should be performed to achieve high interface quality with ALD-Al_2O_3 using TMA as an Al precursor.

Results and discussion

Fig. 1(a) shows the transfer curves of IGZO and fluorinated IGZO (IGZO:F) TFTs measured at drain voltages (V_{DS}) of 1 V and 10 V. The threshold voltage (V_{TH}) was extracted as the gate voltage (V_{GS}) when the drain current was $W/L \times 100$ pA. The subthreshold swing (SS) was defined by the slope of $dV_{GS}/d \log I_{DS}$. The on-current (I_{ON}) was determined as the drain current at $V_{GS} = V_{TH} + 1$ V. With a negative V_{TH} shift of ~4.9 V, the IGZO:F TFT exhibited a lower SS and higher I_{ON} than IGZO TFT. To further validate the impact of our F-PDT process, the NBS test

was conducted as a representative evaluation. Fig. 1(b) shows the NBS results at a V_{GS} of −10 V, equivalent to −1.5 MV cm^{-1}, for 3600 s, where the net V_{TH} shifts for IGZO TFT and IGZO:F TFT were −2.5 V and −0.05 V, respectively.

There are two mechanisms if F is introduced into IGZO: oxygen substitution and V_O passivation.[13,14] The former releases, but the latter consumes electrons, making the resistivity of the thin film lower and higher, respectively. To analyze the energy band structure of the IGZO thin film after F-PDT, UV-vis and UPS characterizations were performed. The optical bandgap was determined from the Tauc plot, and for IGZO and IGZO:F it was 3.52 eV and 3.54 eV, respectively (Fig. 2(a)). Taking the UPS spectra together in Fig. 2(b), the energy band diagrams of the IGZO and IGZO:F thin films are shown in Fig. 2(c). The difference between the conduction band minimum (CBM) and the Fermi level was smaller in the IGZO:F thin film. This implies preferential oxygen substitution over V_O passivation in our study, supporting the negative shift of V_{TH} in Fig. 1(a). Under the NBS conditions, near the interface with the dielectric, the probability of V_O generation from O is high,[33] and the V_Os are more stable in a positively ionized state than a neutral state based on first-principles calculations.[33] These positively charged species are then trapped at the interface, giving rise to the negative shift of V_{TH}. Therefore, the improved NBS stability reflects the oxygen substitution and V_O passivation by F, followed by more stable M–F bond formation.

Next, we investigated whether the F can block H diffusion from the Al_2O_3 into IGZO, because the H plays multiple roles and thereby influences the electrical properties and stability of the TFT. For this purpose, 10 nm-thick Al_2O_3 was grown by a separate thermal ALD system using ozone (O_3) gas, an H-absent oxidant, simply to compare the H concentration. Due to differences in equipment design, the lowest achievable substrate temperature was 180 °C. The TOF–SIMS profiles of as-prepared Al_2O_3/IGZO stacks indicate that the substrate temperature tuning was more effective in modulating the H-associated concentrations than oxidant modification (Fig. S2(a and b), ESI†). The process at a substrate temperature of 150 °C using H_2O oxidant (black), which was our ALD-Al_2O_3 recipe for TFT fabrication, possessed the highest H-associated concentrations of ALD-Al_2O_3, followed by significant diffusion into the IGZO. However, given the negligible difference in H-associated concentrations, the F could not function as a barrier against H diffusion (Fig. S2(c and d), ESI†).
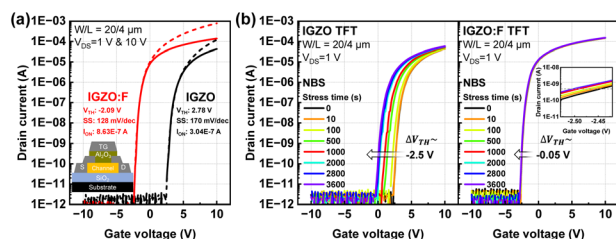

Fig. 1 (a) The transfer curves of IGZO and IGZO:F TFTs measured at V_{DS} of 1 V and 10 V. The device structure and electrical parameters are shown in the inset. (b) The NBS results of IGZO TFT (left) and IGZO:F TFT (right) measured at room temperature. The V_{GS} and V_{DS} were −10 V and 0 V, respectively, for stress conditions. The inset in the right panel shows the enlarged transfer curve near the threshold region.
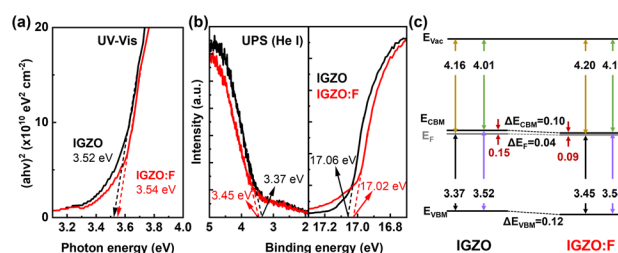

Fig. 2 (a) Tauc plots, (b) UPS spectra, and (c) energy band diagrams of IGZO and IGZO:F thin films.
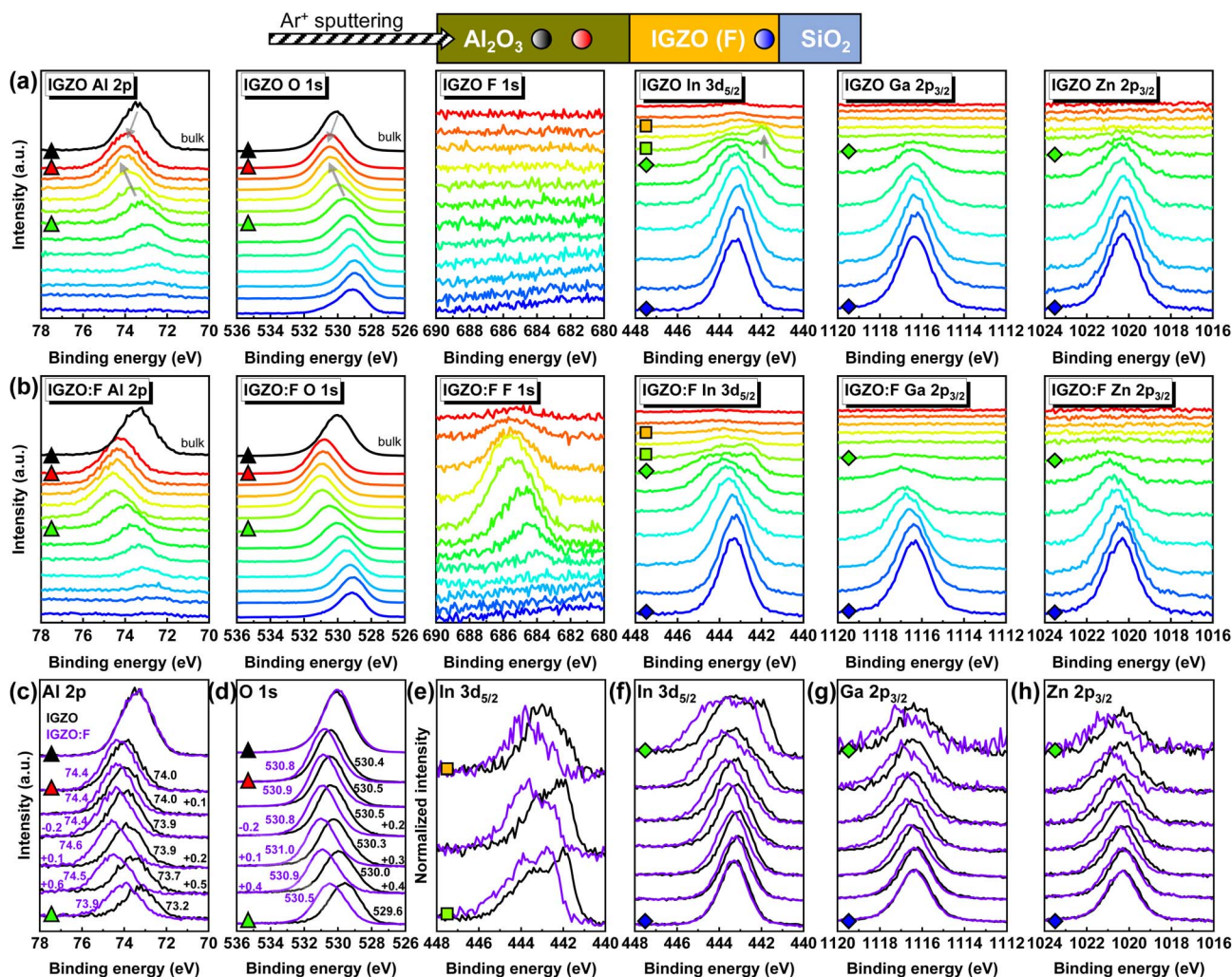
© 2023 The Author(s). Published by the Royal Society of Chemistry

Fig. 3 Depth-resolved XPS core level raw spectra of (a) Al_2O_3/IGZO and (b) Al_2O_3/IGZO:F stacks after the same Ar^+ sputtering time representing Al_2O_3 at the bulk (black), Al_2O_3 near the interface (red), and IGZO at the bottom (blue). (c–h) XPS core level raw spectra of elements to compare the impact of F-PDT marked with colored symbols that are the same as in (a and b). (c) Al 2p and (d) O 1s spectra at bulk Al_2O_3 and near the interface. (e) In $3d_{5/2}$ spectra near the interface. (f) In $3d_{5/2}$, (g) Ga $2p_{3/2}$, and (h) Zn $2p_{3/2}$ spectra from the interface to the bottom IGZO. The depth-resolved XPS spectra in (c–h) represent the relative depth of each Al_2O_3/IGZO (black) and Al_2O_3/IGZO:F (purple) stack, rather than an exact one-to-one depth comparison between the samples.

Fig. 3 shows the depth-resolved XPS core level raw spectra of Al, O, F, In, Ga, and Zn for Al_2O_3/IGZO (F) stacks near the interface. Since the Ar^+ ion sputtering was performed from the Al_2O_3 surface, the Al 2p and O 1s spectra obtained at the bulk position are displayed in black. The color maps represent the relative depth of the stacks: from Al_2O_3 near the interface (red) to IGZO at the bottom (blue). For the Al_2O_3/IGZO stack in Fig. 3(a), upon getting closer to the interface, the Al 2p and O 1s peaks shifted toward higher binding energy (BE), marked with gray arrows, whereas no prominent shift was observed for other metals (In, Ga, and Zn). However, a pronounced shoulder peak at low BE appeared only in the In $3d_{5/2}$ spectra as the position approached the interface. The peak shift toward higher BE in the O 1s spectra near the interface with ALD-Al_2O_3,[30,31] the shoulder peak,[28,32] and/or the peak shift[30–32] in the metal core level spectra of the underlying metal oxides were the key features in the 2DEG phenomenon induced by the TMA. In

other words, the peak shifts in Al 2p and O 1s, and the shoulder peak of In $3d_{5/2}$ in Fig. 3(a) are attributed to the chemical reaction of the IGZO surface during the ALD-Al_2O_3 process. In the case of the quaternary oxide IGZO, the chemical reactions between TMA and all the metal (In, Ga, and Zn) oxides were supposed to be spontaneous based on the thermodynamic calculations.[20] In the experiments, the IGZO thin film and IGZO stack covered by ALD-Al_2O_3 using TMA were compared, and the reduction of the In and Ga species was proposed based on the BE shift toward lower oxidation states (0.13 eV and 0.16 eV for In $3d_{5/2}$ and Ga $3d_{5/2}$, respectively) according to the XPS surface analysis because of extremely thin Al_2O_3 (~2 nm).[20] If the IGZO was covered by a metallic Al (~5 nm) film, which was oxidized into Al_2O_3 after annealing, the reduction of In ions was solely identified through the presence of shoulder peaks in the In 3d doublet spectra.[34] The Ga and Zn spectra were not presented in the literature, with the statement that no obvious change was

found.[34] In our case, we conducted XPS depth profiling of the IGZO stack covered by thick Al_2O_3 (~66 nm) and highlight the shoulder peak in In $3d_{5/2}$ spectra as further straightforward evidence for the reduction of In ions. For other metals, the Ga $2p_{3/2}$ and Zn $2p_{3/2}$ core level spectra at the bottom IGZO were defined as standards and compared with those at upper positions because no significant shoulder peaks were observed in Fig. 3(a). Due to the differences in the composition with respect to the sample depth, the Ga $2p_{3/2}$ and Zn $2p_{3/2}$ spectra were normalized (Fig. S3(a–d), ESI†). The change in the peak BE values for both Ga $2p_{3/2}$ and Zn $2p_{3/2}$ spectra was hard to perceive. A weak sub-peak of Ga $2p_{3/2}$ at low BE was noticed in the top region, but we believe this cannot confirm the chemical reduction because of noise induced by weak raw intensity. In summary, in the standard Al_2O_3/IGZO stack, the TMA was oxidized (higher oxidation state) by scavenging O bonding with In near the IGZO surface at the initial stage of the ALD process, driving the peak shifts of the Al 2p and O 1s spectra toward higher oxidation states. At the same time, the In ions were chemically reduced (lower oxidation state) by TMA, being the origin of the shoulder peak at low BE in the In $3d_{5/2}$ spectra near the interface. Consequently, it is deduced that the standard Al_2O_3/IGZO stack in the absence of F-PDT involves interfacial defects of V_O and interstitial In (In_i).

Fig. 3(b) shows the depth-resolved XPS core level raw spectra of the Al_2O_3/IGZO:F stack. The F 1s peak exhibited a higher intensity when approaching the interface. Considering that our full-width half-maximum (FWHM) of the normalized F 1s core level spectra having the high peak intensity was estimated to be ~3.1 eV (Fig. S3(e and f), ESI†), it is challenging to speculate on the chemical states (see peak BE and FWHM values for In–F, Zn–F, Ga–F, and Al–F bonds in ref. 35). Instead, spectra analysis of the other elements is more beneficial. Fig. 3(c) and (d) compare the Al 2p and O 1s core level spectra with the BE values at the peak positions to emphasize the impact of F-PDT. At the bulk Al_2O_3, both the Al 2p and O 1s spectra were nearly the same, meaning that the difference in the chemical states for Al and O are almost indistinguishable regardless of the F-PDT. On the other hand, when approaching the interface, the Al 2p and O 1s peaks shifted toward higher oxidation states than those in the Al_2O_3/IGZO stack. This is not because of an accelerated redox reaction between the IGZO surface and TMA, but due to the chemical shift by F, which has the highest electronegativity and strong oxidizing nature, consistent with the F introduced into Al_2O_3.[36] In other words, the F forms bonds with O and Al. Besides, the native defects of Al_2O_3 in the proximity of the interface can be occupied by F. In the detailed analysis of Fig. 3(c) and (d), at a depth away from the interface, the peak positions continuously shifted toward higher BE and then were saturated or decreased. For the standard Al_2O_3/IGZO stack, the maximum BE shifts were 0.8 eV and 0.9 eV for Al 2p and O 1s, respectively. On the other hand, for the Al_2O_3/IGZO:F stack, the peak position rapidly shifted toward higher BE because of F and then decreased faster, giving rise to the maximum BE shifts of 0.7 eV and 0.5 eV for Al 2p and O 1s, respectively. This indicates that F-PDT interrupts the reducing behavior of TMA, which scavenges oxygen from the IGZO surface. This is also supported

by the normalized In $3d_{5/2}$ core level spectra near the interface as shown in Fig. 3(e). The shoulder peak observed in the standard Al_2O_3/IGZO stack was still present despite the F-PDT; however, the lower contribution of low oxidation states was obvious. Therefore, it is inferred that the oxidizing agent F, supplied after IGZO deposition, participates in a chemical reaction with the reducing agent TMA during ALD, alleviating the reduction of In ions and decreasing the number of interfacial defects (V_O and In_i). This supports the decrease of the SS and improved stability achieved by IGZO:F TFT in Fig. 1.

Given the above results, the simplest way to counteract the oxygen-scavenging behavior of TMA is to provide supplementary oxygen on the IGZO surface right after its deposition (e.g., post-deposition annealing in air). Another promising approach is to use nitrous oxide (N_2O) plasma treatment that has been conducted for mass production.[37] Note that N_2O exhibits a lower bond order than the diatomic O_2 molecule, having a bond order of 2.[38] Indeed, the chemical reduction reactions of the underlying IGZO were alleviated as a result of N_2O plasma treatment before the ALD-Al_2O_3 process.[20]

As mentioned earlier, the V_O passivation mechanism has previously been suggested in IGZO with the introduction of F. In particular, it has been confirmed theoretically by first-principles calculations based on density functional theory.[39] In experimental work, it is typical to compare by deconvoluting the XPS O 1s core level spectra into three chemical states at a given BE with little tolerance: metal–oxygen (M–O), oxygen-deficient (V_O), and hydroxyl group (–OH).[15,16,40] However, the O 1s spectra were not deconvoluted in this study, considering several issues in the XPS: secondary chemical shift,[41] poor reliability of charge referencing by adventitious carbon (AdC),[41,42] and uncertainty of the BE value assignment for the V_O chemical state in the metal oxides.[43]

Besides the interface with the dielectric, C-related impurities in oxide semiconductors can have a detrimental effect on the stability.[44] In our samples, no distinct C 1s peak was observed in the IGZO or near the interface, even after the F-PDT using CF_4 gas on the IGZO (Fig. S4, ESI†). Regarding the other components of the IGZO upon F-PDT, the normalized core level spectra of all metals (In, Ga, and Zn) are presented in Fig. 3(f–h). The peak BE values near the interface were higher than those in the case of a standard Al_2O_3/IGZO stack, and then converged to the same values as those closer to bottom IGZO. In other words, the F atoms are likely to be concentrated at the interface with a Gaussian-like distribution, extending to the bottom IGZO, which has a thickness of ~10 nm. All metals (In, Ga, and Zn) primarily establish bonds with O at the bottom IGZO and partially with F at the top IGZO. Consequently, the high stability of IGZO:F TFT in Fig. 1(b) was also realized by the stable M–F bond formation at the front channel.

Fig. 4(a and b) show enlarged XPS depth profiles near the Al_2O_3/IGZO (F) interfaces. The F atoms were highly concentrated at the interface, giving rise to the maximum atomic composition of 8.2 at%. It is worth noting that the composition of the interface was In-rich but Ga- and Zn-poor, independent of the F-PDT. This can be attributed to the highest reactivity of TMA with In species, inducing out-diffusion of In toward the
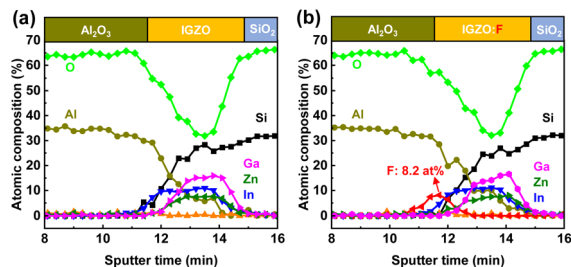
Fig. 4 Enlarged XPS depth profiles of (a) Al_2O_3/IGZO and (b) Al_2O_3/IGZO:F stacks near the interface.

interface. From our In $3d_{5/2}$ core level spectra showing the shoulder peak even in the case of the Al_2O_3/IGZO:F stack, the out-diffusion of In could still happen. In addition, the IGZO (F) layers exhibited considerable Al concentration. Nevertheless, further characterization is required to validate these speculations if considering the thickness of the IGZO (F) thin films (~10 nm) and the principles behind the XPS depth profiling. Taking our case for example, after sputtering the sample in the vertical direction using an Ar^+ ion gun (2 keV), X-ray photons emitted by an Al Kα (1486.6 eV) source penetrate into the sample, and the kinetic energies of photoexcited electrons that leave the elements of interest are detected. These sequential procedures are performed repeatedly, collecting narrow-scan spectra of elements as a function of Ar^+ sputtering time. One should take into account the (1) atomic mixing during the Ar^+ ion sputtering and (2) photoionization cross section and probing depth (typically shorter than 10 nm) of the elements during the XPS analysis.[41] The ion bombardment can make surface atoms stick into the film, so atoms at shallow and deep positions are intermixed. In addition, the kinetic energies of photoelectrons from the elements at both shallow and deep positions can be detected simultaneously due to the probing depth. Accordingly, depth-resolved elemental profiles at the interface derived from XPS data may not reflect the precise distributions. To make sure our data were reliable, we conducted (scanning) TEM analysis and EDS line scanning along the interface, to obtain elemental information on the vertically stacked sample in the lateral direction.

Cross-sectional TEM bright-field (BF) images in Fig. 5(a and b) show the rough Al_2O_3/IGZO interface in contrast with the sharp Al_2O_3/IGZO:F interface. This fully agrees with the depth-resolved XPS analysis that the defect (V_O and In_i)-rich Al_2O_3/

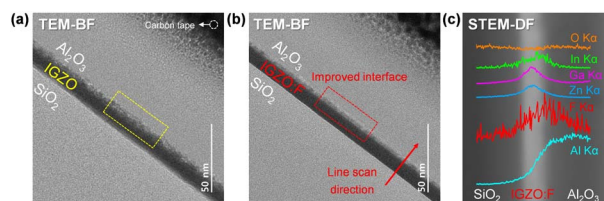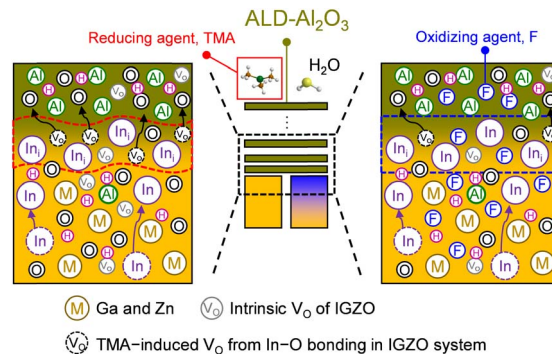**Fig. 6** Schematic of F-PDT on the ALD-Al_2O_3/IGZO stack.

IGZO interface was improved as a result of F-PDT because the reduction of In ions vulnerable to the reducing agent TMA was hindered by the oxidizing agent F. Moreover, the EDS line scan profiles in Fig. 5(c) present coherent information that we have inferred from Fig. 4: (i) F atoms concentrated at the Al_2O_3/IGZO:F interface with Gaussian-like distributions, (ii) In–rich interface, and (iii) Al diffusion into IGZO.

Conclusions

Fig. 6 shows a schematic of the result of F-PDT on IGZO and its relationship with the subsequent ALD-Al_2O_3 process. At the initial stage of the ALD process, a strong reducing agent, TMA itself, was oxidized by scavenging O, particularly bonding with In at the IGZO surface. This resulted in a rough and defect-rich (V_O and In_i) interface between the Al_2O_3 and IGZO, examined by TEM and depth-resolved XPS, respectively. We employed F, known as a stability enhancer, by substituting O and passivating V_O. Given the chemical shifts in the depth-resolved XPS results, stable M–F bond formation was observed for all metals (In, Ga, and Zn), whereas F could not function as a barrier against H diffusion during low-temperature ALD-Al_2O_3. Nevertheless, F with strong oxidizing character alleviated the chemical reduction reaction of the IGZO surface, establishing a sharp and defect-passivated interface. In summary, a high interface quality was obtained as a result of oxidizing agent supply before the ALD-Al_2O_3 process. Consequently, improved electrical properties and stability were realized by the top gate TFT configuration. We highlight that, to secure excellent interface quality, the post-deposition oxidation of the IGZO surface should be performed before ALD-Al_2O_3 process using TMA as a metal precursor.

Experimental

TFT fabrication

A thermally grown SiO_2/Si substrate was cleaned by acetone, IPA and DI water for 15 min each. After RF sputtering of IGZO (~10 nm) using a 4-inch ceramic target (In : Ga : Zn = 1 : 1 : 1 at%, purity: 4 N) under Ar/O_2 (60/1 sccm) plasma, diluted HCl was used for channel patterning. The F-PDT was performed based on CF_4/O_2 (100/2 sccm) gas for 15 s at a RF bias of 1700 W. The

Fig. 5 Cross-sectional TEM bright-field (BF) images of (a) Al_2O_3/IGZO and (b) Al_2O_3/IGZO:F stacks. (c) Scanning TEM (STEM) dark-field (DF) image of the Al_2O_3/IGZO:F stack with raw EDS line scan data.

working pressures for IGZO deposition and F-PDT were 5 and 20 mTorr, respectively. E-beam evaporated Ti/Ni stacks were used as S/D electrodes. Next, Al_2O_3 (~66 nm) was prepared by a traveling wave type thermal ALD at a growth temperature of 150 °C using TMA and H_2O as a metal precursor and oxidant, respectively. After TG (e-beam evaporated Ti/Ni stacks) patterning and subsequent Al_2O_3 wet etching, the device was annealed by a hot plate at 180 °C for 1 h. All processes were conducted at room temperature except for the ALD and annealing steps. The device structure is shown in the inset of Fig. 1.

Characterization

The electrical properties of the TFTs were measured using a semiconductor parameter analyzer (4200-SCS, Keithley) under ambient conditions and representative parameters were extracted at a V_{DS} of 1 V. Time-of-flight secondary ion mass spectrometry (TOF-SIMS; TOF SIMS 5, ION-TOF) was performed using a primary ion source of Bi^+ (30 keV, 1 pA) and a sputtering source of Cs^+ (1 keV, 70 nA). The Tauc plots of the thin films were obtained by an ultraviolet-visible (UV-vis; U-2900, Hitachi) spectrophotometer. Ultraviolet photoelectron spectroscopy (UPS; Versaprobe III, PHI) was utilized to quantify the secondary electron cutoff energy and work function using a He I (21.22 eV) source after IGZO surface etching. The atomic compositions and chemical states were analyzed by XPS (Versaprobe III, PHI) using an Al Kα (1486.6 eV) source with Ar^+ ion sputtering at an acceleration voltage of 2 keV. Adventitious carbon (AdC) was detected at the sample surface, and the peak BE values for In, Ga, and Zn core level spectra after charge referencing by AdC at 284.8 eV agreed well with the NIST database (Fig. S1, ESI†).[45] Nevertheless, in this work, we discuss the BE shifts and features of core level raw spectra with respect to sample depth, rather than focusing on the absolute BE values, because of the uncertainty of charge referencing by AdC.[41,42] The chemical shifts are supported by the literature and energy-dispersive spectroscopy (EDS) data, measured by TEM (JEM-2100F, JEOL Ltd) at 200 kV. A focused ion beam (FIB) (Helios 5 UC, FEI) was used for sample preparation.

Conflicts of interest

The authors declare no conflict of interest.

Acknowledgements

References

1 S. Park, S. Seong, G. Jeon, W. Ji, K. Noh, S. Kim and Y. Chung, *Adv. Electron. Mater.*, 2023, **9**, 2200554.

2 Y. H. Chen, I. T. Wang, Y. M. Zheng and T. H. Hou, *presented in part at the 2023 7th IEEE Electron Devices Technology & Manufacturing Conference (EDTM)*, March, 2023.

3 M. R. Sk, S. Thunder, D. Lehninger, S. Sanctis, Y. Raffel, M. Lederer, M. P. M. Jank, T. Kämpfe, S. De and B. Chakrabarti, *ACS Appl. Electron. Mater.*, 2023, **5**, 812–820.

4 A. Belmonte, H. Oh, S. Subhechha, N. Rassoul, H. Hody, H. Dekkers, R. Delhougne, L. Ricotti, K. Banerjee, A. Chasin, M. J. v. Setten, H. Puliyalil, M. Pak, L. Teugels, D. Tsvetanova, K. Vandersmissen, S. Kundu, J. Heijlen, D. Batuk, J. Geypen, L. Goux and G. S. Kar, *presented in part at the 2021 IEEE International Electron Devices Meeting (IEDM)*, Dec, 2021.

5 Y. Zhang, J. Li, J. Li, T. Huang, Y. Guan, Y. Zhang, H. Yang, M. Chan, X. Wang, L. Lu and S. Zhang, *Adv. Electron. Mater.*, 2023, **9**, 2300150.

6 A. Belmonte, H. Oh, N. Rassoul, G. L. Donadio, J. Mitard, H. Dekkers, R. Delhougne, S. Subhechha, A. Chasin, M. J. v. Setten, L. Kljucar, M. Mao, H. Puliyalil, M. Pak, L. Teugels, D. Tsvetanova, K. Banerjee, L. Souriau, Z. Tokei, L. Goux and G. S. Kar, *presented in part at the 2020 IEEE International Electron Devices Meeting (IEDM)*, Dec, 2020.

7 C. Chen, X. Duan, G. Yang, C. Lu, D. Geng, L. Li and M. Liu, *presented in part at the 2022 IEEE International Electron Devices Meeting (IEDM)*, Dec, 2022.

8 K. Huang, X. Duan, J. Feng, Y. Sun, C. Lu, C. Chen, G. Jiao, X. Lin, J. Shao, S. Yin, J. Sheng, Z. Wang, W. Zhang, X. Chuai, J. Niu, W. Wang, Y. Wu, W. Jing, Z. Wang, J. Xu, G. Yang, D. Geng, L. Li and M. Liu, *presented in part at the 2022 IEEE Symposium on VLSI Technology and Circuits (VLSI Technology and Circuits)*, June, 2022.

9 M. S. Kim, H. T. Kim, H. Yoo, D. H. Choi, J. W. Park, T. S. Kim, J. H. Lim and H. J. Kim, *ACS Appl. Mater. Interfaces*, 2021, **13**, 31816–31824.

10 Y. Jang and S.-Y. Lee, *ACS Appl. Electron. Mater.*, 2023, **5**, 509–519.

11 J. W. Choi, J. Kim, S. R. Pae, J. Kim, C. G. Kim, H. Lee, S. Ji, S.-W. Nam, Y. K. Lee and B. Shin, *Chem. Mater.*, 2022, **34**, 6802–6808.

12 A. Zakutayev, *J. Mater. Chem. A*, 2016, **4**, 6742–6754.

13 S. Lee, J. Shin and J. Jang, *Adv. Funct. Mater.*, 2017, **27**, 1604921.

14 J. Jiang, T. Toda, M. P. Hung, D. Wang and M. Furuta, *Appl. Phys. Express*, 2014, **7**, 114103.

15 L. Lu, Z. Xia, J. Li, Z. Feng, S. Wang, H. S. Kwok and M. Wong, *IEEE Electron Device Lett.*, 2018, **39**, 196–199.

16 M. Miyakawa, M. Nakata, H. Tsuji, H. Iino and Y. Fujisaki, *AIP Adv.*, 2020, **10**, 065004.

17 K.-M. Jung, J. Oh, H. E. Kim, A. Schuck, K. Kim, K. Park, J.-H. Jeon, S.-Y. Lee and Y.-S. Kim, *J. Phys. D: Appl. Phys.*, 2020, **53**, 355107.

18 S. Wang, J. Li, R. Shi, Z. Xia, L. Lu, H. S. Kwok and M. Wong, *J. Soc. Inf. Disp.*, 2020, **28**, 520–527.

19 W. Pan, Y. Wang, Y. Wang, Z. Xia, F. S. Y. Yeung, M. Wong, H. S. Kwok, X. Wang, S. Zhang and L. Lu, *J. Alloys Compd.*, 2023, **947**, 169509.

20 J. Li, Y. Zhang, J. Wang, H. Yang, X. Zhou, M. Chan, X. Wang, L. Lu and S. Zhang, *ACS Appl. Mater. Interfaces*, 2023, **15**, 8666–8675.

21 D.-G. Kim, W.-B. Lee, S. Lee, J. Koh, B. Kuh and J.-S. Park, *ACS Appl. Mater. Interfaces*, 2023, **15**, 36550–36563.

22 J. K. Lee, S. An and S. Y. Lee, *IEEE Electron Device Lett.*, 2023, **44**, 1845–1848.

23 J. Yang, H. Park, B. Kim, Y.-H. Cho and S.-H. K. Park, *J. Mater. Chem. C*, 2022, **10**, 9699–9706.

24 J. Park, Y. Jang, J. Lee, S. An, J. Mok and S.-Y. Lee, *Adv. Electron. Mater.*, 2023, **9**, 2201306.

25 J. Kim, T. H. Kim, S. Oh, J. H. Nam, H. Y. Jang, Y. Kim, N. Yamada, H. Kobayashi, S.-Y. Kim, B. H. Lee, H. Habazaki, W. Park and B. Cho, *ACS Appl. Electron. Mater.*, 2020, **2**, 1478–1483.

26 C. Guerra-Nuñez, M. Döbeli, J. Michler and I. Utke, *Chem. Mater.*, 2017, **29**, 8690–8703.

27 H. J. Lee, T. Moon, S. D. Hyun, S. Kang and C. S. Hwang, *Adv. Electron. Mater.*, 2021, **7**, 2000876.

28 T. J. Seok, Y. Liu, J. H. Choi, H. J. Kim, D. H. Kim, S. M. Kim, J. H. Jang, D.-Y. Cho, S. W. Lee and T. J. Park, *Chem. Mater.*, 2020, **32**, 7662–7669.

29 T. J. Seok, Y. Liu, H. J. Jung, S. B. Kim, D. H. Kim, S. M. Kim, J. H. Jang, D.-Y. Cho, S. W. Lee and T. J. Park, *ACS Nano*, 2018, **12**, 10403–10409.

30 X. Zhu, T. Zhang, Y. He, Y. Liu and H. Zhu, *Nanoscale*, 2023, **15**, 12071–12077.

31 Z. Zhu, T. Yasui, X. Zhao, Q. Liu, S. Morita, Y. Li, A. Yonezu, K. Nagashima, T. Takahashi, M. Osada, R. Matsuda, T. Yanagida and Y. Baba, *ACS Appl. Mater. Interfaces*, 2023, **15**, 36866–36876.

32 S. Y. Lee, J. Kim, A. Park, J. Park and H. Seo, *ACS Nano*, 2017, **11**, 6040–6047.

33 A. de Jamblinne de Meux, A. Bhoolokam, G. Pourtois, J. Genoe and P. Heremans, *Phys. Status Solidi A*, 2017, **214**, 1600889.

34 H. Yang, X. Zhou, H. Fu, B. Chang, Y. Min, H. Peng, L. Lu and S. Zhang, *ACS Appl. Mater. Interfaces*, 2021, **13**, 11442–11448.

35 Y. Kawamoto, K. Ogura, M. Shojiya, M. Takahashi and K. Kadono, *J. Fluorine Chem.*, 1999, **96**, 135–139.

36 S. Lee, D. I. Kim, M. Kim, M. Son, W. Song, S. Myung, H.-K. Jung, S. S. Lee, D. H. Yoon, S. Yim and K.-S. An, *Appl. Surf. Sci.*, 2023, **630**, 157464.

37 H. Kim, C. Han, D. Kim and B. Choi, *IEEE Trans. Electron Devices*, 2023, **70**, 3611–3616.

38 R. D. Harcourt and A. Schulz, *J. Phys. Chem. A*, 2000, **104**, 6510–6516.

39 H. Kawai, H. Fujiwara, J. Kataoka, N. Saito, T. Ueda, T. Enda, T. Ishihara and K. Ikeda, *presented in part at the 2020 IEEE International Electron Devices Meeting (IEDM)*, Dec, 2020.

40 J. G. Um and J. Jang, *Appl. Phys. Lett.*, 2018, **112**, 162104.

41 G. Greczynski and L. Hultman, *J. Appl. Phys.*, 2022, **132**, 011101.

42 G. Greczynski and L. Hultman, *Prog. Mater. Sci.*, 2020, **107**, 100591.

43 T. J. Frankcombe and Y. Liu, *Chem. Mater.*, 2023, **35**, 5468–5474.

44 Y.-S. Shiah, K. Sim, Y. Shi, K. Abe, S. Ueda, M. Sasase, J. Kim and H. Hosono, *Nat. Electron.*, 2021, **4**, 800–807.

45 *NIST X-ray Photoelectron Spectroscopy Database, NIST Standard Reference Database Number 20*, DOI: **10.18434/T4T88K**, **https://srdata.nist.gov/xps/**.